Acta Crystallographica Section F
Structural Biology and Crystallization Communications
ISSN 1744-3091

Engineered tryptophan in the adenine-binding pocket of catalytic subunit A of A-ATP synthase demonstrates the importance of aromatic residues in adenine binding, forming a tool for steady-state and time-resolved fluorescence spectroscopy

Vikeramjeet Singh Tadwal, Malathy Sony Subramanian Manimekalai and Gerhard Grüber*

School of Biological Sciences, Nanyang Technological University, 60 Nanyang Drive, Singapore 637551, Singapore

Correspondence e-mail: ggrueber@ntu.edu.sg

Received 7 July 2011
Accepted 27 September 2011

PDB References: subunit A of A-ATP synthase, F427W mutant, 3sdz; F508W mutant, 3se0.

A reporter tryptophan residue was individually introduced by site-directed mutagenesis into the adenine-binding pocket of the catalytic subunit A (F427W and F508W mutants) of the motor protein A_1A_O ATP synthase from *Pyrococcus horikoshii* OT3. The crystal structures of the F427W and F508W mutant proteins were determined to 2.5 and 2.6 Å resolution, respectively. The tryptophan substitution caused the fluorescence signal to increase by 28% (F427W) and 33% (F508W), with a shift from 333 nm in the wild-type protein to 339 nm in the mutant proteins. Tryptophan emission spectra showed binding of Mg-ATP to the F427W mutant with a K_d of 8.5 μ*M*. In contrast, no significant binding of nucleotide could be observed for the F508W mutant. A closer inspection of the crystal structure of the F427W mutant showed that the adenine-binding pocket had widened by 0.7 Å (to 8.70 Å) in comparison to the wild-type subunit A (8.07 Å) owing to tryptophan substitution, as a result of which it was able to bind ATP. In contrast, the adenine-binding pocket had narrowed in the F508W mutant. The two mutants presented demonstrate that the exact volume of the adenine ribose binding pocket is essential for nucleotide binding and even minor narrowing makes it unfit for nucleotide binding. In addition, structural and fluorescence data confirmed the viability of the fluorescently active mutant F427W, which had ideal tryptophan spectra for future structure-based time-resolved dynamic measurements of the catalytic subunit A of the ATP-synthesizing enzyme A-ATP synthase.

1. Introduction

Archaea are very different from bacteria and eukarya with respect to physiology, which allows them to withstand extremely harsh conditions, but they employ similar chemiosmotic mechanisms for energy conservation (Müller *et al.*, 2005). The archaeal ATP synthases known as A_1A_O ATP synthases are key enzymes in their energy metabolism. These enzymes are evolutionarily closely related to V_1V_O ATPases from eukarya, but are only distantly related to F_1F_O ATP synthases from bacteria. However, their function is more similar to those of F_1F_O ATP synthases as they are used by the cells to produce ATP, in sharp contrast to the V_1V_O ATPases (Grüber *et al.*, 2001; Grüber & Marshansky, 2008). As described for bacterial F_1F_O ATP synthases (subunits α_3:β_3:γ:λ:ε:*a*:b_2:c_x) and eukaryotic V_1V_O ATPases (subunits A_3:B_3:C:D:E:F:G_2:H_x:*a*:*d*:*c*:*c*′:*c*″), A_1A_O ATP synthases (subunits A_3:B_3:C:D:E:F:H_2:*a*:c_x) consist of a water-soluble A_1 part, which contains the catalytic sites, and a membrane-embedded A_O part, which is involved in ion translocation (Boekema *et al.*, 1999; Böttcher & Gräber, 2000; Coskun, Chaban *et al.*, 2004; Coskun, Radermacher *et al.*, 2004). These parts are connected through a central stalk (subunits C, D and F) and two peripheral stalks containing subunits E and H and the N-terminus of subunit *a* (Grüber & Marshansky, 2008; Chaban *et al.*, 2002; Gayen *et al.*, 2007; Lee *et al.*, 2010). A-ATP synthases harness energy from an H^+ and/or an Na^+ gradient, using

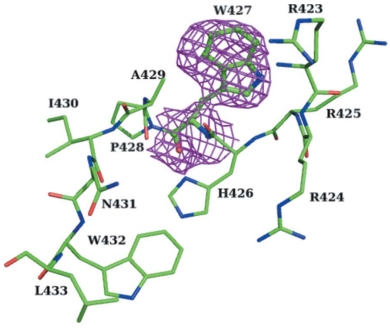

the flux of ions across the membrane *via* the ion channels to drive the synthesis of ATP (Deppenmeier & Müller, 2006).

Subunit A has been proposed to have a catalytic function (Schäfer *et al.*, 2006), while subunit B is regarded to play an important role in the nucleotide-binding and/or regulatory function (Kumar *et al.*, 2009; Manimekalai *et al.*, 2009; Schäfer *et al.*, 2006). The three-dimensional structure of subunit A of A-ATP synthases consists of an N-terminal β-barrel, a unique nonhomologous region (NHR, a stretch of 90 amino acids), a central α–β domain and a C-terminal α-helical bundle (Maegawa *et al.*, 2006; Kumar *et al.*, 2010). Subunit A of A-ATP synthase from *Pyrococcus horikoshii* OT3 contains a conserved P-loop motif ($_{234}$GPFGSGKT$_{241}$, also known as the Walker A motif; Saraste *et al.*, 1990), which interacts with the phosphate groups of the nucleotide (Kumar *et al.*, 2010). Although no sequence motif has been reported for adenine binding in nucleotide-binding proteins (Kuttner *et al.*, 2003; Denessiouk *et al.*, 2001), the adenine pocket is mainly comprised of hydrophobic residues above and below the adenine and polar residues at the border (Kuttner *et al.*, 2003; Moodie *et al.*, 1996). As described in the AMP-PNP-bound crystal structure of subunit A of A-ATP synthase from *P. horikoshii* OT3 (Kumar *et al.*, 2010), the aromatic residues Phe427 and Phe508 stabilize the adenine moiety by sandwiching the adenine from both sides by establishing π–π interactions. In order to analyze and understand the role of residues Phe427 and Phe508 in adenine stability and nucleotide binding of subunit A, a tryptophan has been specifically introduced at these locations by site-directed mutagenesis, serving as a direct probe of nucleotide binding in the catalytic subunit A. The crystal structures of the F427W and F508W mutant proteins were determined to resolutions of 2.5 and 2.6 Å, respectively, giving insight into the adenine-binding pocket of subunit A and the positions of the introduced tryptophan residues relative to the adenine ring.

2. Materials and methods

2.1. Construction and purification of F427W and F508W mutants of subunit A

The F427W mutant construct was generated by the overlap extension polymerase chain reaction (PCR) method (Ho *et al.*, 1989) using subunit A inserted into pET22b(+) as a template (Kumar *et al.*, 2010). In separate PCR reactions, two fragments of the target sequence were amplified by using one flanking primer (*a* or *d*) and one mutagenic primer (*b* or *c*) in each reaction. The flanking primers were 5′-GAG-GTG-AGT-A**CA**-**TAT**-**G**GT-GGC-GAA-GGG-GAG-3′ (forward primer *a*) incorporating an *Nde*I restriction site (bold) and 5′-CTT-GCT-CA**G**-**TCG**-**AC**T-CAC-GCC-CCA-TAC-TTC-3′ (reverse primer *d*) with a *Sal*I restriction site (bold). The mutagenic primers with mismatched bases (bold) were 5′-GAC-TTA-GCT-AGG-AGA-AGA-CAC-**TGG**-AAC-GCA-ATC-AAC-TGG-TTG-3′ (mutagenic forward primer *b*) and 5′-CAA-CCA-GTT-GAT-TGC-TGG-**CCA**-GTG-TCT-TCT-CCT-AGC-TAA-GTC-3′ (mutagenic reverse primer *c*). The two intermediate products with terminal complementarity were gel-purified and used to generate a new template DNA by duplexing in a second reaction. During the overlap extension phase, the fused product was amplified using the two original flanking primers (*a* and *d*). A similar strategy was employed to construct the F508W mutant of subunit A using the internal mutagenic primers 5′- GAT-TAT-CTA-CAG-CAG-GAT-GCC-**TGG**-GAT-GAA-GTA-GAT-ACC-TAC-TG-3′ (mutagenic forward primer *b*) and 5′-C-AGA-GGT-ATC-TAC-AAC-ATC-**CCA**-GGC-ATC-CTG-CTG-TAG-ATA-ATC-3′ (mutagenic reverse primer *c*) with mismatched bases shown in bold and using the same flanking primers as described for the F427W mutant. The resulting full-length mutant gene fragments were then cleaved with *Nde*I/*Sal*I restriction enzymes and ligated into a pET22b(+) vector. The mutant DNA was sequenced and transformed into *Escherichia coli* BL21 CodonPlus (DE3)-RIL cells (Stratagene) for protein expression using the electroporation method and spread onto LB agar plates containing ampicillin (100 µg ml^{-1}) and chloramphenicol (34 µg ml^{-1}). Single colonies were used to inoculate a 100 ml primary culture, which was subsequently used to inoculate a 4 l secondary culture in LB medium containing appropriate antibiotics. Cells were grown and harvested and the mutant proteins were purified according to Kumar *et al.* (2010). The purity was analyzed by SDS–PAGE (Laemmli, 1970). Protein concentrations were determined using the bicinchonic acid assay (BCA; Pierce, Rockford, Illinois, USA).

2.2. Crystallization, data collection and structure determination

Crystallization screens were set up for the mutant subunit A proteins using the hanging-drop vapour-diffusion method according to Kumar *et al.* (2010). The mutant proteins were crystallized from a solution consisting of 0.1 *M* acetate pH 4.5 and 35%(*v*/*v*) MPD as precipitant at 291 K. The rate of diffusion was decreased by overlaying a 1:1 mixture of paraffin and silicone oil onto the mother liquor to a final volume of 200 µl, which yielded high-quality crystals. For the cocrystallization trials with nucleotides, the purified mutant proteins were split into three portions and incubated separately with 2 m*M* Mg-ATP, 2 m*M* Mg-ADP or 2 m*M* Mg-AMP-PNP at 277 K for 30 min on a sample rotator. These mixtures were then concentrated to 10–12 mg ml^{-1} using 50 kDa Centricon concentrators (Amicon). The protein–ligand complexes were set up for crystallization using the same optimized conditions in hanging-drop plates as described above. Diffraction-quality crystals of the F427W mutant were obtained in the absence or presence of Mg-ATP or Mg-ADP. In contrast, diffracting crystals of the F508W mutant only grew in the absence or presence of Mg-AMP-PNP.

Data sets for the F427W and F508W subunit A mutants were collected at 100 K on beamline 13B1 at the National Synchrotron Radiation Research Center (NSRRC, Hsinchu, Taiwan) using an ADSC Quantum 315 CCD detector. Crystals of the F427W mutant grown in the presence of Mg-ATP, in the presence of Mg-ADP and in the absence of nucleotide diffracted to resolutions of 2.9, 2.6 and 2.5 Å, respectively. In the case of the F508W mutant, crystals grown in the absence of nucleotide and in the presence of MgAMP-PNP diffracted to resolutions of 2.6 and 2.9 Å, respectively. The data were indexed, integrated and scaled using the *HKL*-2000 suite (Otwinowski & Minor, 1997). All crystals belonged to the tetragonal space group $P4_32_12$ and had similar unit-cell parameters.

The structure of subunit A from *P. horikoshii* OT3 (PDB entry 1vdz; Maegawa *et al.*, 2006) was used as a model for structure determination by the molecular-replacement method using the program *Phaser* (McCoy *et al.*, 2007). Initially, rigid-body refinement was carried out followed by the calculation of difference Fourier syntheses. Inspection of the $F_o - F_c$ and $2F_o - F_c$ maps for the protein–nucleotide complexes clearly showed that nucleotides were not present in the complex crystals for both mutants. Since no nucleotide-bound forms could be observed in the analysed crystals, the best data set with the highest resolution was chosen for further structure analysis for both mutants. For the F427W mutant (2.5 Å resolution) as well as the F508W mutant (2.6 Å resolution), diffraction data sets from the nucleotide-free form were used for structure determination. Iterative cycles of model building and restrained refinement were carried out using the programs *Coot* (Emsley &

Cowtan, 2004) and *REFMAC*5 (Murshudov *et al.*, 2011) from the *CCP*4 suite (Winn *et al.*, 2011) to improve the phases. Refinement was performed until convergence and TLS (Translation, Liberation and Screw) restraints were included in the final cycles of refinement. The domain definitions were determined using the *TLS Motion Determination* server (Painter & Merritt, 2006). The quality of the refined model was validated using the program *PROCHECK* (Laskowski *et al.*, 1993) and the figures were generated using the program *PyMOL* (DeLano, 2002). Structural comparison analysis was carried out using the *SUPERPOSE* program (Krissinel & Henrick, 2004) as implemented in the *CCP*4 suite. Details of the data-collection and refinement statistics are given in Table 1.

2.3. PDB codes

Atomic coordinates and structure factors for the F427W and F508W subunit A mutants have been deposited in the RCSB Protein Data Bank under accession codes 3sdz and 3se0, respectively.

2.4. Fluorescence measurements

A Varian Cary Eclipse spectrofluorometer was used and all experiments were carried out at 293 K. The samples were excited at 295 nm and emission was recorded from 310 to 380 nm with excitation and emission band passes set to 5 nm. For nucleotide titration of the tryptophan fluorescence of subunit A and its F427W and F508W mutants the emission wavelength was 338 nm. Before titration, the mutant protein and increasing amounts of Mg-ATP were incubated in 50 m*M* Tris–HCl pH 7.5 buffer for 5 min on ice.

3. Results and discussion

3.1. Crystallographic structures of the F427W and F508W mutants of subunit A

The F427W and F508W mutant proteins were crystallized as elaborated in Kumar *et al.* (2010) and their structures were determined to final resolutions of 2.5 and 2.6 Å, respectively. The initial phases were obtained by molecular replacement using the wild-type subunit A (WT-A) structure from *P. horikoshii* OT3 (PDB entry 1vdz; Maegawa *et al.*, 2006) as a model. The phases were then improved by multiple cycles of manually adjusting the model into the electron density and by performing restrained refinement until convergence. The final structure showed good geometry and stereochemistry, as demonstrated in Table 1. The mutation was clearly visible in the electron-density map, which fitted perfectly to the corresponding mutated residue (Fig. 1).

In the crystal structure of the F427W mutant the N-terminal residues from Met25 to Val59 could be identified and assigned (Fig. 2). The final model has good stereochemistry and includes 549 amino acids, six MPD molecules, six acetate molecules, three tris(hydroxymethyl)aminomethane (Tris) molecules and 293 water molecules. There is no interpretable density for residues 1–24 and 340–355 in the electron-density map of the F427W mutant and thus these segments are missing in the final model. The final refined model of the F508W mutant includes 519 amino acids, one sulfate ion, three MPD molecules, one Tris molecule and 142 water molecules. No interpretable density could be identified for residues 1–63 and 346–350 and therefore these residues are missing from the final model. The detailed statistics of data collection, phasing and structure refinement for both mutants are given in Table 1. The additionally identified residues in the N-terminal region of mutant F427W are disordered but still form a separate N-terminal domain constituted of residues 25–79, 110–116 and 189–199. The other three domains, *i.e.* the NHR (residues 117–188), the nucleotide-binding α–β domain (residues 80–99 and 200–437) and the C-terminal α-helical bundle (residues 438–588), are well defined. The P-loop region ($_{234}$GPFGSGKT$_{241}$) in the F427W mutant is highly disturbed and these residues could be assigned from the positive peaks in the difference Fourier map ($F_o - F_c$) during the structure-refinement procedure. The P-loop acquires a flat relaxed conformation in comparison to the arched wild-type (WT) conformation (Supplementary Fig. S1[1]). The arched conformation of the WT-A P-loop is mainly held in place by direct interaction of Phe236 with the side chains of Asp331 and Glu244, direct interaction of the side chain of Pro235 with the main chain of Ser238 and indirect association of the side chains of Asp331 and Glu267 with Gly237 *via* a water molecule (Kumar *et al.*, 2010). In comparison, in the F427W mutant structure the direct interaction of Pro235 and Ser238, as well as the interactions of Phe236 with Asp331 and Glu244, are abolished, indicating that the substitution by tryptophan has interrupted the concerted main interactions formed by the critical P-loop residues Pro235, Phe236 and Ser238.

Table 1
Crystallographic and refinement statistics of the F427W and F508W mutant subunit A proteins from *P. horikoshii* OT3.

Values in parentheses are for the highest resolution shell.

	F427W	F508W
Data-collection statistics		
Wavelength (Å)	1.0	1.0
Space group	$P4_32_12$	$P4_32_12$
Unit-cell parameters (Å)		
$a = b$ (Å)	127.88	128.54
c (Å)	105.50	103.86
$\alpha = \beta = \gamma$ (°)	90	90
Resolution range (Å)	26.2–2.53 (2.62–2.53)	29.8–2.62 (2.71–2.62)
Solvent content (%)	62.61	62.09
No. of unique reflections	29815	26796
$\langle I/\sigma(I)\rangle$	37.04 (3.8)	38.7 (3.9)
Completeness (%)	99.9 (100)	99.8 (100)
R_{merge}† (%)	5.3 (46.2)	5.6 (62.7)
Multiplicity	7.9 (8.0)	9.7 (9.9)
Refinement statistics		
R factor‡ (%)	19.97	22.68
R_{free}§ (%)	26.58	27.21
No. of amino-acid residues	544	519
No. of water molecules	293	142
No. of MPD molecules	6	3
No. of acetate molecules	6	2
No. of Tris molecules	3	1
Ramachandran statistics		
Most favoured (%)	85.6	87.6
Additionally allowed (%)	12.0	11.0
Generously allowed (%)	2.4	1.4
Disallowed (%)	0	0
R.m.s. deviations		
Bond lengths (Å)	0.02	0.01
Bond angles (°)	1.95	1.31
Mean atomic B values (Å^2)		
Overall	60.32	65.15
Wilson plot	62.74	69.27

† $R_{merge} = \sum_{hkl}\sum_i |I_i(hkl) - \langle I(hkl)\rangle| / \sum_{hkl}\sum_i I_i(hkl)$, where $\langle I(hkl)\rangle$ is the mean intensity of reflection hkl. ‡ R factor $= \sum_{hkl} ||F_{obs}| - |F_{calc}|| / \sum_{hkl} |F_{obs}|$, where F_o and F_c are the measured and calculated structure factors, respectively. § $R_{free} = \sum_{hkl} ||F_{obs}| - |F_{calc}|| / \sum_{hkl} |F_{obs}|$ calculated from 5% of the reflections that were randomly selected and omitted during refinement.

3.2. Structural comparison of the F427W mutant with WT-A

Comparison of the F427W mutant structure with that of the WT-A protein (PDB entry 3i72; Kumar *et al.*, 2010) was performed by

[1] Supplementary material has been deposited in the IUCr electronic archive (Reference: BE5183).

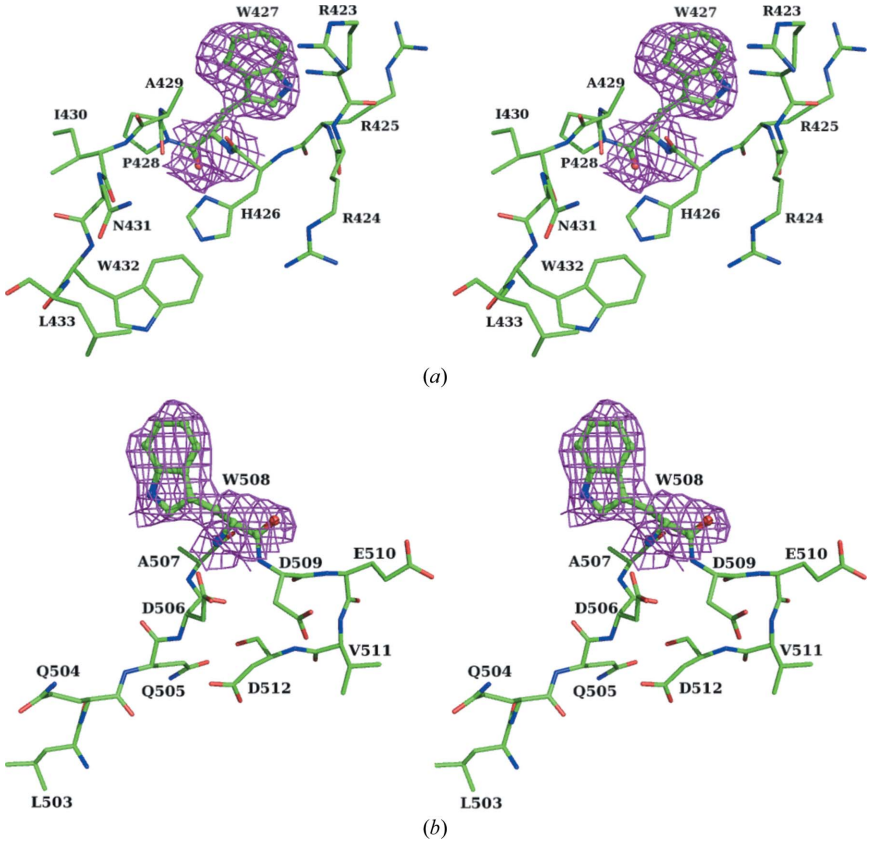

Figure 1
Stereoview of an OMIT map ($F_o - F_c$) contoured at 2.0σ (magenta) showing the mutations at F427W (*a*) and F508W (*b*) of the A subunit of the A_1A_O ATP synthase from *P. horikoshii* OT3. The OMIT map was calculated by removing the mutant residues (either Trp427 or Trp508) and then randomly displacing the final coordinates of the mutant structures by 0.3 Å using *MOLEMAN*2. The resultant coordinates were refined by *REFMAC* for 25 cycles, which gave an unbiased map.

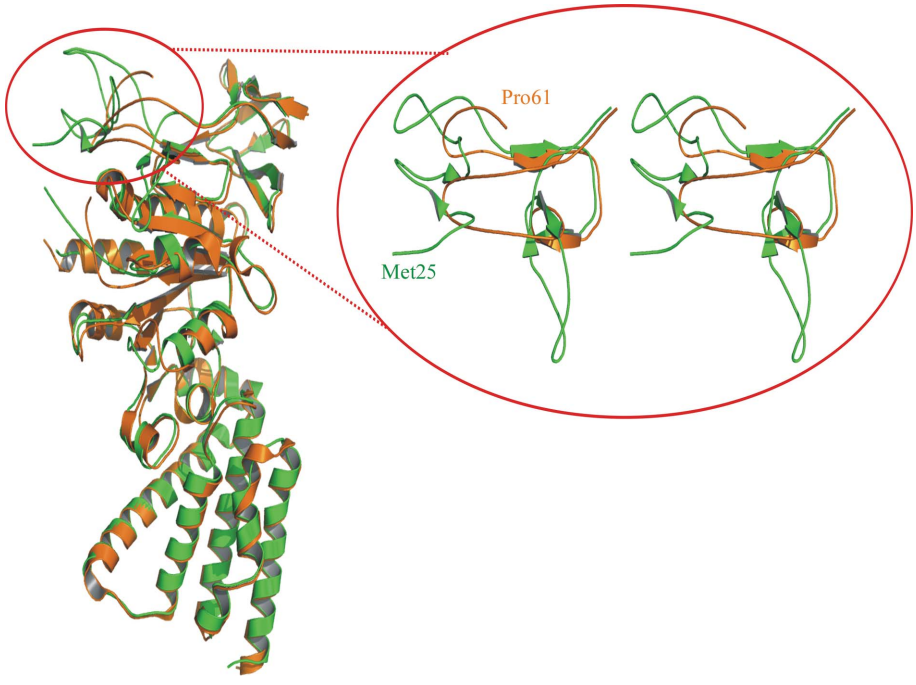

Figure 2
Structural overlap of the F427W mutant (green) with the WT A subunit of A_1A_O ATP synthase from *P. horikoshii* (PDB entry 3i72; orange; Kumar *et al.*, 2010). The inset shows a stereoview of the additionally assigned residues in the F427W mutant structure, displaying the additional secondary structure as β-sheets. The N-terminal loop region from Val94 to Val107 makes a rotation of around 84.7° in the opposite direction. The first residue in the F427W mutant is Met25 and that in WT-A is Pro61.

superimposing the structures, which yielded an r.m.s. deviation of 0.66 Å for the backbone C^{α} atoms of the core regions containing 478 residues (Fig. 2*a*). Greater than average deviations were noted for the following segments: Val94–Val107 (maximum deviation of 20.56 Å occurring for Asp101), Pro235–Thr241 (maximum deviation of 7.82 Å occurring for Phe236) and Thr333–Tyr359 (maximum deviation of 9.54 Å occurring for Ala339). The N-terminal loop region from Val92 to Val107 shows a major deviation, with a large movement of this loop region, which makes a rotation of around 84.7° in the opposite direction. This movement could be ascribed to the assignment of the N-terminal residues Met25–Val59 in the F427W mutant structure; this region was previously occupied by a loop in the wild-type structure (Fig. 2). This loop region was previously misinterpreted in WT-A because of the missing 60 N-terminal residues (Maegawa *et al.*, 2006). The larger deviation in this segment is also reflected by high flexibility in this region: the average *B* factor for this segment is 108.49 $Å^2$. The segment Thr333–Tyr356 falls in the discontinuous region and therefore greater deviations than average are observed. Residues Phe427 and Phe508 in AMP-PNP-bound WT-A sandwich the adenine moiety from both sides by forming a π–π interaction (Kumar *et al.*, 2010) and the distance between these two residues (Phe427 and Phe508) is 8.07 Å. In comparison, in the F427W mutant the corresponding residues are 8.70 Å apart when superimposed with the AMP-PNP-bound WT-A structure (Fig. 3). The distances are measured from the centroids of the respective rings in the residues. The angle between the least-square planes of the rings of residues Trp427 and Phe427 when the F427W mutant is superimposed with the WT-A subunit is 13.6°, suggesting movement away of residue Trp427 in the mutant F427W. This widening of the nucleotide-binding region owing to the tryptophan substitution may explain the P-loop disturbances observed in the F427W mutant. In comparison with the WT-A structure, the F427W mutant only undergoes alterations in the

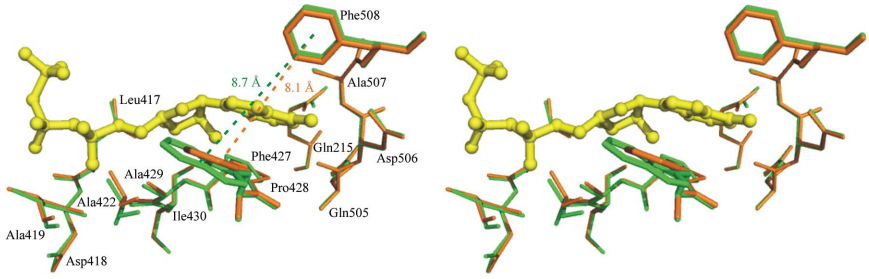

Figure 3
Comparison of the adenine-binding pocket regions of the AMP-PNP-bound WT A subunit (orange; PDB entry 3i72; Kumar *et al.*, 2010; APP-PNP is shown in a yellow ball-and-stick representation) and the F427W mutant (green) in stereoview showing the variation in the orientation of the residues owing to the mutation of Phe to Trp at site 427. The distances between residues 427 and 508 in both the F427W mutant and the WT A subunit are measured from the centroids of the respective residues (dotted lines) with the adenine ring of the AMP-PNP molecule in the WT-A structure.

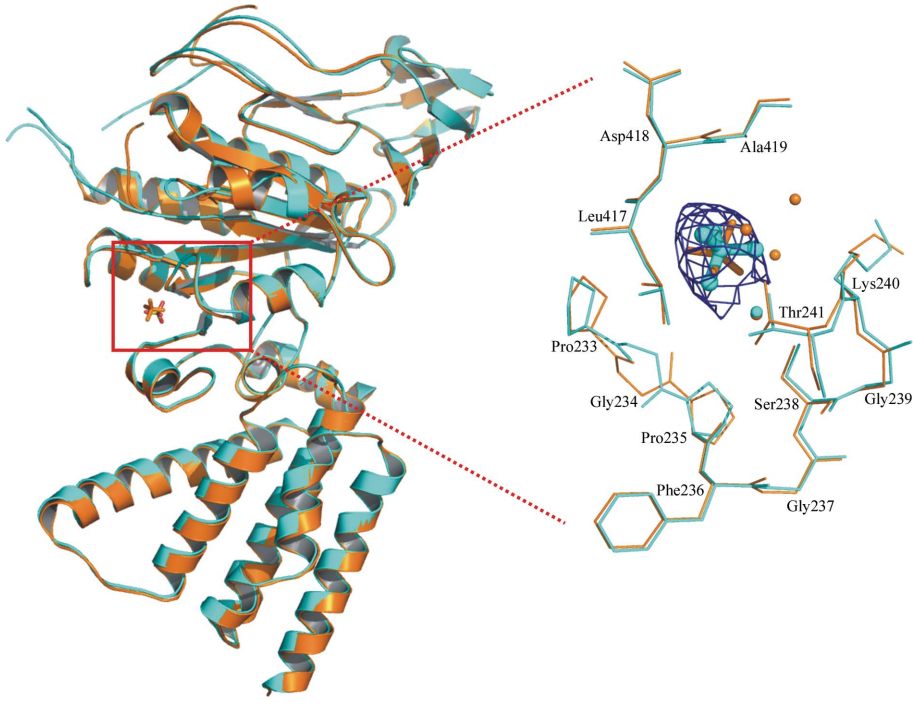

Figure 4
(*a*) Structural overlap of the WT A subunit (PDB entry 3i72; Kumar *et al.*, 2010; orange) with the F508W mutant (cyan). (*b*) Binding region within a 5 Å radius of the sulfate molecule and the P-loop residues ($_{234}$GPFGSGKT$_{241}$). The sulfate (cyan ball-and-stick representation) $F_o - F_c$ electron-density map contoured at the 3.0σ level is shown in blue for the F508W mutant, while the amino-acid residues surrounding it are shown in stick representation. The sulfate molecule of the WT A subunit is displayed as sticks (orange). Water molecules for the F508W mutant are shown in cyan and those for the Wt A subunit are shown in orange.

N-terminal domain and the nucleotide-binding domain; the NHR domain and the C-terminal α-helical domain do not show much deviation.

3.3. Superposition of the F508W mutant with WT-A

The F508W mutant superimposes with the WT A subunit (PDB entry 3i72; Kumar *et al.*, 2010) with an r.m.s.d. of 1.13 Å for the backbone C^{α} atoms. Greater deviations than average were observed for the regions Arg96–Pro110 (3.55 Å for Ile103), Cys261–Val271 (5.01 Å for Asn266) and Ser334–Tyr356 (9.48 Å for Ala339). As observed for the F427W mutant, the loop region Arg96–Pro110 does not show any large movements. The P-loop region ($_{234}$GPFG-SGKT_{241}) has retained the similar arched conformation as found in the WT A subunit. The P-loop and the nearby loop (Val391–Glu401) in the F508W mutant are at the same distance as in the WT A subunit (19 Å). The segment Cys261–Val271 includes the GER-loop ($_{262}$GER_{264}) and perturbations in the side-chain arrangements of these residues might have led to the positioning of this loop at 9.7 Å from the P-loop in the mutant F508W in comparison to the distance of 7.9 Å in the WT A subunit. Also, the GER-loop has moved away by 3.8 Å in comparison to the WT A subunit. The region Ser334–Tyr356 belongs to the break region and deviation is noticed as expected.

A sulfate ion which arises from the precipitating agent could be observed in the electron-density map of the F508W mutant. The sulfate molecule may interact with two P-loop segment ($_{234}$GPFG-SGKT_{241}) residues, Ser238 and Thr241, *via* a single water molecule (Fig. 4). This is similar to the WT A subunit, where it binds to the P-loop region by a single residue (Ser238) through a water molecule (Kumar *et al.*, 2010). The water-bridge interactions in both the F508W mutant and the WT A subunit are well stabilized in the structures. The interactions of the sulfate molecule with various residues within 5 Å radius as well as with the P-loop residues in both the F508W mutant and WT A subunits are shown in Fig. 4. The position of the sulfate ion in the structure of the F508W mutant is different and has moved away from the P-loop by an average of around 0.9 Å in comparison to the WT A subunit. However, the position of the sulfate ion in terms of location in the F508W mutant is between the β- and γ-phosphate of the AMP-PNP molecule and is similar to that in the WT A subunit.

3.4. Fluorescence properties of the F427W and F508W subunit A mutants

The reporter tryptophan residue engineered at the critical location in the adenine-binding pocket in the F427W and F508W mutants of subunit A yielded increases of 28 and 33% in the fluorescence intensity in the nucleotide-free form compared with WT-A, respectively (Fig. 5*a*), indicating the contribution of the introduced tryptophan residue. Relative to the wavelength position of the wild-type spectrum, with a maximum at 339 nm, the spectra of both mutants were red-shifted, with a maximum at 333 nm, indicating a hydrophobic environment. The addition of 2 m*M* Mg-ATP to nucleotide-depleted F427W mutant resulted in a quenching of 28% and a shift of the fluorescence signal of the mutant protein, making the spectrum of the F427W mutant similar to that of WT-A (Fig. 5*a*).

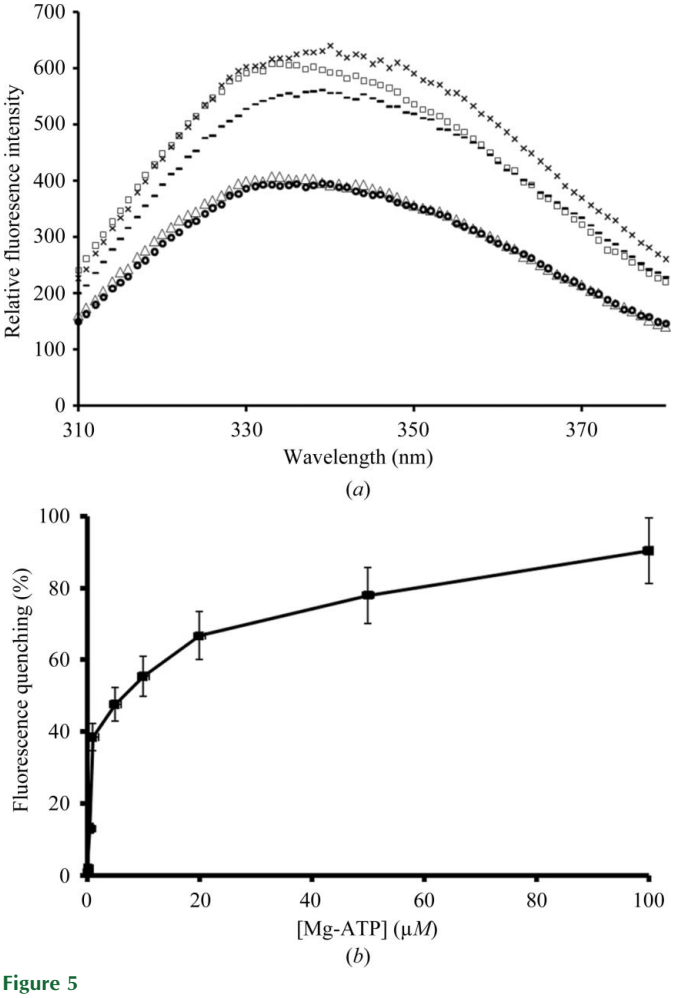

Figure 5
(*a*) Tryptophan fluorescence spectra of WT A subunit (circles), the F427W mutant (lines) and the F508W mutant (squares). The fluorescence spectrum of the F427W (triangles) and F508W (crosses) mutants of subunit A in the presence of 2 m*M* Mg-ATP are also shown. An equimolar ratio of Mg^{2+} to ATP was used in the experiments. The proteins were diluted in 50 m*M* Tris–HCl pH 7.5. The emission spectra were measured using λ_{em} = 295 nm with emission and excitation slits at 5 nm. (*b*) Fluorescence titration of the F427W mutant protein with Mg-ATP. Excitation and emission were measured at 295 and 333 nm, respectively. Three replicates of the experiments were performed.

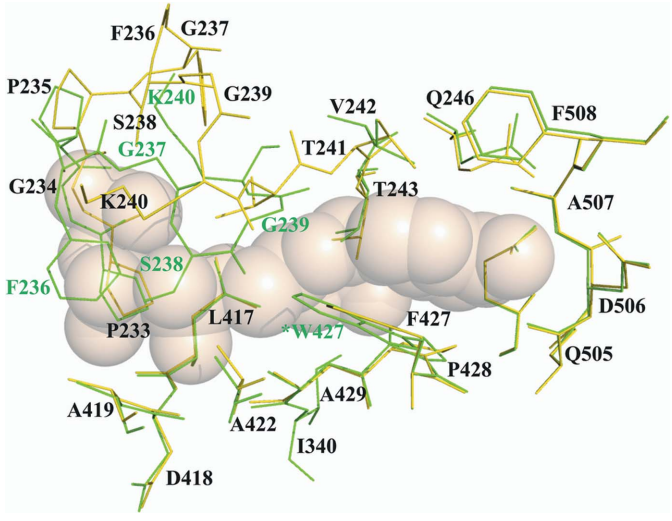

Figure 6
Structural overlap of the AMP-PNP-binding region (within 5 Å) in the AMP-PNP-bound structure of WT-A (yellow; PDB entry 3i4l; Kumar *et al.*, 2010) and the F427W (green; PDB entry 3sdz) mutant structure of subunit A. The AMP-PNP molecule is shown as spheres (in wheat). The mutated residue in the F427W mutant is labelled with an asterisk (*). For clarity, the residues of the AMP-PNP-bound structure of subunit A are labelled. In addition, residues of the F427W mutant showing major deviations are labelled in green.

However, the emission spectrum of the F508W mutant showed a minor increase in quenching upon supplementation with 2 m*M* Mg-ATP. To quantitatively evaluate the fluorescence response of the F427W mutant, the binding of the mutant to an increasing concentration of Mg-ATP was measured using fluorescence quenching at 333 nm and the result is shown in Fig. 5(*b*). The titration curve has a hyperbolic shape, from which a binding constant (K_d) of 8.5 $\pm$ 3 µ*M* could be determined. This value is comparable to the K_d of 2.38 µ*M* measured for the WT protein by isothermal titration calorimetry (Kumar *et al.*, 2010).

3.5. Contribution of residues Phe427 and Phe508 in the adenine-binding pocket

Comparison of the adenine ribose-binding pockets of the F427W and F508W mutants with the AMP-PNP-bound structure of subunit A revealed that even though most of the surrounding residues are very similar, alterations are noted for the residues at positions 427 and 508 (Fig. 6 and Supplementary Fig. S2). In the F427W mutant the distance (calculated from the centroids of the rings) between residues 427 and 508 is increased (8.7 Å), while in the F508W mutant this distance is similar (8.1 Å) in comparison to the AMP-PNP-bound structure of subunit A (8.2 Å). Furthermore, the plane of the tryptophan ring (at location 427) of the F427W mutant deviates by about 10° outwards in comparison to the phenylalanine ring (at location 427) of the AMP-PNP-bound structure of subunit A, thereby moving away from residue Phe508 and widening the angle between them (to about 80°). The angle is measured between the least-square planes of the rings. In contrast, for the F508W mutant this angle deviates by approximately 14° inwards for residue 508, resulting in an orientation which brings Trp508 closer to Phe427 and thereby decreases the angle between the two residues by about 15° (to around 57°) when compared with the AMP-PNP-bound structure (around 72°). Taken together, the adenine-binding pocket has widened in the F427W mutant owing to an increased distance (0.7 Å) and tilt (around 10°) of the rings of residue 427, while in the F508W mutant it is narrowed by around 15°. This widening of the adenine-binding pocket in the structure of the F427W mutant might allow free movement of nucleotides, whereas this movement is hindered in the F508W mutant owing to the narrowed nucleotide-binding pocket. Hence, this structural perturbation explains the ability of the F427W mutant to bind to Mg-ATP and the inability of the F508W mutant to bind to Mg-ATP, as observed from the tryptophan fluorescence measurements. The two mutants, F427W and F508W, clearly demonstrate that the exact volume of the adenine-ribose binding pocket is essential for nucleotide binding and any minor narrowing would make it unfit for nucleotide binding. Furthermore, the fluorescently active F427W mutant, with its ideal tryptophan spectrum, now opens a new avenue for future structure-based time-resolved dynamic measurements (von Feilitzsch *et al.*, 2008) of the catalytic A subunit of the energy-conserving enzyme A-ATP synthase.

We thank the staff of beamline 13B1 at the National Synchrotron Radiation Research Centre (NSRRC), a national user facility supported by the National Science Council of Taiwan, ROC, for expert help with data collection. The Synchrotron Radiation Protein Crystallography Facility at NSRRC is supported by the National Research Program for Genomic Medicine. VST thanks the Nanyang Technological University for the award of a research scholarship. This research was supported by A*STAR BMRC (06/1/22/19/467).

References

Boekema, E. J., van Breemen, J. F., Brisson, A., Ubbink-Kok, T., Konings, W. N. & Lolkema, J. S. (1999). *Nature (London)*, **401**, 37–38.
Böttcher, B. & Gräber, P. (2000). *Biochim. Biophys. Acta*, **1458**, 404–416.
Chaban, Y., Ubbink-Kok, T., Keegstra, W., Lolkema, J. S. & Boekema, E. J. (2002). *EMBO Rep.* **3**, 1–10.
Coskun, Ü., Chaban, Y. L., Lingl, A., Müller, V., Keegstra, W., Boekema, E. J. & Grüber, G. (2004). *J. Biol. Chem.* **279**, 38644–38648.
Coskun, Ü., Radermacher, M., Müller, V., Ruiz, T. & Grüber, G. (2004). *J. Biol. Chem.* **279**, 22759–22764.
DeLano, W. L. (2002). *PyMOL*. http://www.pymol.org.
Denessiouk, K. A., Rantanen, V. V. & Johnson, M. S. (2001). *Proteins*, **44**, 282–291.
Deppenmeier, U. & Müller, V. (2006). *Results Probl. Cell Differ.* **45**, 123–152.
Emsley, P. & Cowtan, K. (2004). *Acta Cryst.* D**60**, 2126–2132.
Feilitzsch, T. von, Tuma, J., Neubauer, H., Verdier, L., Haselsberger, R., Feick, R., Gurzadyan, G., Voityuk, A. A., Griesinger, C. & Michel-Beyerle, M. E. (2008). *J. Phys. Chem. B*, **112**, 973–989.
Gayen, S., Vivekanandan, S., Biuković, G., Grüber, G. & Yoon, H. S. (2007). *Biochemistry*, **46**, 11684–11694.
Grüber, G. & Marshansky, V. (2008). *Bioessays*, **30**, 1096–1109.
Grüber, G., Svergun, D. I., Coskun, Ü., Lemker, T., Koch, M. H., Schägger, H. & Müller, V. (2001). *Biochemistry*, **40**, 1890–1896.
Ho, S. N., Hunt, H. D., Horton, R. M., Pullen, J. K. & Pease, L. R. (1989). *Gene*, **77**, 51–59.
Krissinel, E. & Henrick, K. (2004). *Acta Cryst.* D**60**, 2256–2268.
Kumar, A., Manimekalai, M. S., Balakrishna, A. M., Hunke, C., Weigelt, S., Sewald, N. & Grüber, G. (2009). *Proteins*, **75**, 807–819.
Kumar, A., Manimekalai, M. S., Balakrishna, A. M., Jeyakanthan, J. & Grüber, G. (2010). *J. Mol. Biol.* **396**, 301–320.
Kuttner, Y. Y., Sobolev, V., Raskind, A. & Edelman, M. (2003). *Proteins*, **52**, 400–411.
Laemmli, U. K. (1970). *Nature (London)*, **227**, 680–685.
Laskowski, R. A., MacArthur, M. W., Moss, D. S. & Thornton, J. M. (1993). *J. Appl. Cryst.* **26**, 283–291.
Lee, L. K., Stewart, A. G., Donohoe, M., Bernal, R. A. & Stock, D. (2010). *Nature Struct. Mol. Biol.* **17**, 373–378.
Maegawa, Y., Morita, H., Iyaguchi, D., Yao, M., Watanabe, N. & Tanaka, I. (2006). *Acta Cryst.* D**62**, 483–488.
Manimekalai, M. S., Kumar, A., Balakrishna, A. M. & Grüber, G. (2009). *J. Struct. Biol.* **166**, 38–45.
McCoy, A. J., Grosse-Kunstleve, R. W., Adams, P. D., Winn, M. D., Storoni, L. C. & Read, R. J. (2007). *J. Appl. Cryst.* **40**, 658–674.
Moodie, S. L., Mitchell, J. B. & Thornton, J. M. (1996). *J. Mol. Biol.* **263**, 486–500.
Müller, V., Lemker, T., Lingl, A., Weidner, C., Coskun, U. & Grüber, G. (2005). *J. Mol. Microbiol. Biotechnol.* **10**, 167–180.
Murshudov, G. N., Skubák, P., Lebedev, A. A., Pannu, N. S., Steiner, R. A., Nicholls, R. A., Winn, M. D., Long, F. & Vagin, A. A. (2011). *Acta Cryst.* D**67**, 355–367.
Otwinowski, Z. & Minor, W. (1997). *Methods Enzymol.* **276**, 307–326.
Painter, J. & Merritt, E. A. (2006). *J. Appl. Cryst.* **39**, 109–111.
Saraste, M., Sibbald, P. R. & Wittinghofer, A. (1990). *Trends Biochem. Sci.* **15**, 430–434.
Schäfer, I. B., Bailer, S. M., Düser, M. G., Börsch, M., Bernal, R. A., Stock, D. & Grüber, G. (2006). *J. Mol. Biol.* **358**, 725–740.
Winn, M. D. *et al.* (2011). *Acta Cryst.* D**67**, 235–242.